

Anomalous diffusion in semi-crystalline polymer structures

E G Kostadinova ¹, J L Padgett ², C D Liaw ^{1, 3}, L S Matthews ¹, & T W Hyde ¹

¹ CASPER and Department of Physics, Baylor University, Waco, TX 76706, USA

² Department of Mathematics and Statistics, Texas Tech University, Lubbock, TX 79409, USA

³ Department of Mathematical Sciences, University of Delaware, Newark, DE 19716, USA

E-mail: Eva_Kostadinova@baylor.edu, joshua.padgett@ttu.edu, liaw@udel.edu,
Lorin_Matthews@baylor.edu, Truell_Hyde@baylor.edu

Abstract. From the spread of pollutants in the atmosphere to the transmission of nutrients across cell membranes, anomalous diffusion processes are ubiquitous in natural systems. The ability to understand and control the mechanisms guiding such processes across various scales has important application to research in materials science, finance, medicine, and energetics. Here we present an analytical method for studying anomalous diffusion which combines concepts from fractional calculus and spectral theory in a model where transport is guided by non-local interactions and random disorder. The proposed technique determines transport properties from the spectrum of an Anderson-type Hamiltonian with a discrete fractional Laplacian operator $(-\Delta)^s$, $s \in (0,2)$ and a random distribution of disorder. We present a physical interpretation of the model in the context of light diffusion through semi-crystalline polymer structures. In this formulation, transport is numerically studied as a function of disorder concentration, characteristics of nonlocal interactions, and vector scales in the Hilbert space. The results show enhanced transport for $s < 1$ (super-diffusion) and enhanced localization for $s > 1$ (sub-diffusion) for most examined cases. An important finding of the present study is that transport can be enhanced at key correlation lengths in the sub-diffusive case, where all states are normally expected to be localized for a disordered system.

Keywords: Anomalous diffusion, fractional Laplacian, spectral approach, semi-crystalline polymers

I. INTRODUCTION

The problem of the random walk, as originally defined by Pearson in 1905 [1], deals with the path generated by a man making straight-line displacements, each with a fixed length and a random direction. If the man forgets all previous directions each time a new displacement is made, the random walk is described by the well-known diffusion equation, proposed by Fick [2] and derived from first principles by Einstein [3]. When many “forgetful” random walkers start from the same origin, the probability distribution function (PDF) of their positions approaches a Gaussian and their mean squared displacement (MSD) increases linearly with time. In the presence of memory (or correlations), the successive displacements of a walker are not fully independent, resulting in anomalous diffusion process with non-Gaussian PDF and a non-linear plot of $MSD(t)$. *Super-diffusion* is commonly described as a random walk where the walker can make big jumps in displacement, called Lévy flights. Such a process can be characterized by a Lévy PDF and MSD that increases faster than linear as a function of time. In contrast, *sub-diffusion* is a process in which the walker’s motion is impeded, leading to an MSD that increases slower than linear as a function of time. Figure 1 provides a visual representation of the characteristic particle trajectories resulting from different choices of a PDF, corresponding to the three diffusion regimes. In each plot, the particle trajectories were generated using numerical techniques from Tarantino et al. [4]. Since various mechanisms can cause sub-diffusion, the corresponding PDF is not unique. Fig. 1c illustrates a case of sub-diffusion where the sub-diffusive trajectories were obtained using a PDF, which is a superposition of truncated Gaussian and Lévy distributions. This choice will be further discussed in Sec. IV.

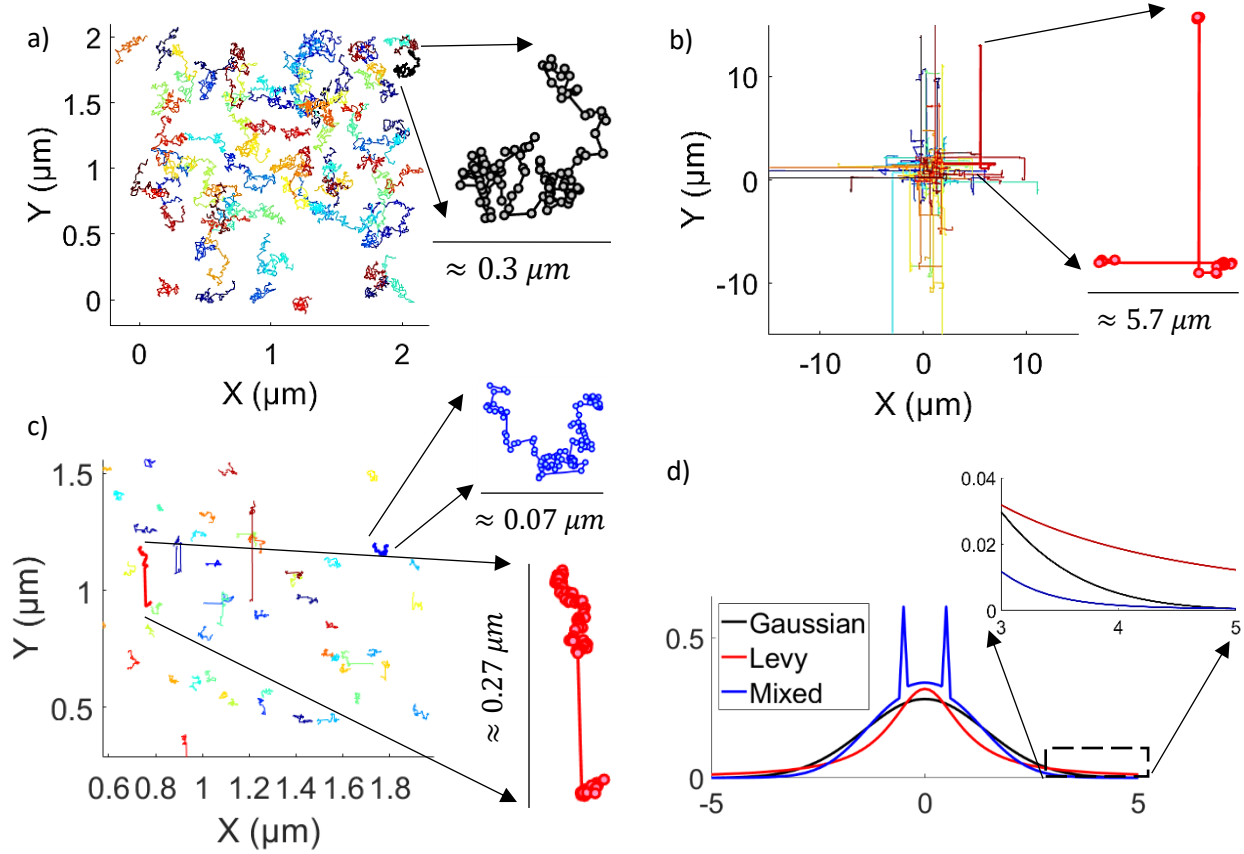


Fig. 1. Typical particle trajectories, representing a) Fickian diffusion, b) super-diffusion, and c) sub-diffusion. Gaussian PDF was used to generate the trajectories in a), while a Lévy PDF was used in b). The trajectories in c) were obtained from a truncated superposition of Gaussian and Lévy PDFs. The three PDFs are superimposed in d).

The ubiquity of anomalous diffusion processes observed in laboratory experiments and in nature is well captured by the words of Klafter and Sokolov [5]: “*although these phenomena are called anomalous, they are abundant in everyday life: anomalous is normal*”. Super-diffusion has been observed in the search patterns of animals [6]–[8], the spread of pollutants in the ocean and the atmosphere [9], [10], and particle transport in turbulent plasmas [11]–[13]. Sub-diffusion has been found characteristic of electron transport in amorphous materials [14], gas transport in porous media [15], signal transmission across cell membranes [16], [17], and protein fluctuation patterns [18]. The variety of natural systems exhibiting anomalous diffusion requires the development of generalized mathematical techniques together with appropriate physical interpretations, adapting such techniques to specific problems. This paper presents a spectral method [19] for studying anomalous diffusion, which combines concepts from fractional calculus and spectral theory in a mathematical model [20] where transport is guided by non-local interactions and random disorder. Although the proofs of this technique are general (applicable to any Anderson-type Hamiltonian [21]), here we apply the model to the problem of light transport in semi-crystalline polymers, which are known to exhibit both disorder and nonlocal interactions [22], [23].

Of specific interest in the present work is extending the theory of Anderson localization to include many-body nonlocal interactions and to investigate the resulting nonlinear (anomalous) transport. Anderson localization describes the absence of diffusion due to lattice impurities (disorder) [24]

and has been examined in various systems, including quantum walkers, Bose-Einstein condensates, photon lattices, and granular chains [25]–[29]. A long-standing question in the theory of Anderson localization is the effect of many-body nonlocal interactions on diffusion in disordered media [30]. Many-body transport has been investigated in fermionic systems at high temperatures, quantum spin chains, weakly-correlated electrons, and granular chains with strongly nonlinear interactions [31]–[34]. The interplay between stochastic disorder and nonlocal interactions can lead to interesting nonlinear dynamics, such as plasma turbulence [12] and the excitation of solitary waves and solitons in soft matter [35], [36]. An important result from studies of one-dimensional granular crystals is that in the presence of disorder and non-linearity, which individually favor localization, the energy transport in the system can be super-diffusive [34], [37].

In the present study, we consider the process of nonlinear (or anomalous) diffusion of light photons due to nonlocal interactions in a semi-crystalline polymer media with Anderson-type random disorder. Nonlocal interactions are modeled using the fractional Laplace operator, which is often employed in the study of anomalous diffusion [38], [39]. The properties of the discrete fractional Laplacian $(-\Delta)^s$, $s \in (0,2)$ were examined in detail in our previous work [20], where we also discussed its application in a spectral approach [19] to the Anderson localization problem. The resulting Fractional Laplacian Spectral (FLS) model was employed in a one-dimensional numerical simulation [20] which demonstrated qualitative transport enhancement in the super-diffusive case, $s \in (0,1)$, and enhanced localization in the sub-diffusive regime, $s \in (1,2)$. Here we extend the application of the FLS technique by examining transport as a function of disorder concentration, range of nonlocality, fractional exponent of the Laplacian, and vector scales in the Hilbert space. These parameters are interpreted as physical properties of a polymer media, such as molecular chain length and orientation.

In Sec. II, we summarize the main theoretical results used as a basis for the FLS model. Section III introduces the problem of light transport through a semi-crystalline polymer and discusses the physical interpretation and application of the FLS technique to this setup. Section IV presents a numerical study of anomalous diffusion for various choices of disorder, range and type of nonlocal interactions, and vector scales in the Hilbert space. A major finding of the present study is the existence of enhanced transport for key combinations of vector scales and range of nonlocality in the sub-diffusive regime. The possible physical origins of these results are discussed in Appendix B, where we also examine numerical instabilities due to roundoff errors and other approximations. Sec. V provides a summary of the results and outlines directions for future research.

II. FRACTIONAL LAPLACIAN SPECTRAL MODEL

In this paper, we extend the 1D Anderson localization problem to include nonlocal interactions by considering the *random fractional discrete Schrödinger operator*

$$H_{s,\epsilon} := (-\Delta)^s + \sum_{i \in \mathbb{Z}} \epsilon_i \langle \cdot, \delta_i \rangle \delta_i, \quad (1)$$

where $(-\Delta)^s$, $s \in (0,2)$ is the discrete fractional Laplacian, δ_i is the i th standard basis vector of the 1D integer space \mathbb{Z} , $\langle \cdot, \cdot \rangle$ is the $\ell^2(\mathbb{Z})$ inner product, and ϵ_i are independent variables, identically distributed according to a uniform distribution on the interval $[-c/2, c/2]$, with $c > 0$. The operator in (1) is appropriate for studying particle transport characterized by nonlocal interactions, such as positive or negative correlations in a many-body disordered system. It is expected that in

the *super-diffusive* regime $s \in (0,1)$, transport is enhanced due to positive correlations, while in the *sub-diffusive* regime $s \in (1,2)$, propagation through the medium slows down due to negative correlations [38], [39]. In the limit where $s \rightarrow 1$, the fractional Laplacian reduces to the classical case. Note that, in our model, the effect of random disorder is considered as a localization mechanism, which is distinct from the effect of negative correlations in the sub-diffusive regime.

Throughout literature, there are numerous definitions of the fractional Laplacian involving singular integrals, semigroups of operators, and harmonic extensions [40]. A common representation in 1D is given by the hyper-singular integral of the form

$$(-\Delta)^s u_n := c_s \lim_{h \rightarrow 0^+} \int_{\mathbb{R} \setminus L_\varepsilon(n)} \frac{u(n) - u(\xi)}{|n - \xi|^{1+2s}} d\xi, \quad (2)$$

where $s \in (0,1)$, $u_n \equiv u(n)$, $n \in \mathbb{Z}$ is a function, and $L_\varepsilon(n)$ is a line segment of length $\varepsilon > 0$ centered at $n \in \mathbb{Z}$, and c_s is a normalization constant. Caffarelli and Silvestre [41] demonstrated that the operator $(-\Delta)^s$, $s \in (0,1)$ can be constructed from a harmonic extension problem to the upper half space as the operator that maps Dirichlet to Neumann boundary conditions. Recently, Chen et al. [42] derived similar extension results for the case $(-\Delta)^s$, $s > 1$. Padgett *et al.* [20] combined these techniques to obtain the following 1D series representation of the fractional Laplacian for $s \in (0,2)$

$$(-\Delta)^s u_n = \sum_{m \in \mathbb{Z}; m \neq n} (u_n - u_m) K_s(n - m), \quad (3)$$

where

$$K_s(m) = \begin{cases} \frac{4^s \Gamma(1/2 + s)}{\sqrt{\pi} |\Gamma(-s)|} \cdot \frac{\Gamma(|m| - s)}{\Gamma(|m| + 1 + s)}, & m \in \mathbb{Z} \setminus \{0\}, \\ 0, & m = 0. \end{cases} \quad (4)$$

Here u is a discrete function of the lattice points in the space, with $u_n \equiv u(n)$, $n \in \mathbb{Z}$ and Γ is the Gamma function. Numerical simulations by Padgett *et al.* [20] provided qualitative confirmation that the representation in (3) yields enhanced transport (super-diffusion) for $s \in (0,1)$ and enhanced localization (sub-diffusion) for $s \in (1,2)$ when compared to the classical case $s = 1$. The present work expands this study by investigating how transport depends on the interplay between disorder concentration and the various characteristics of the nonlocal interactions.

In our model, the transport behavior under the action of the Hamiltonian in (1) is determined from a numerical test, where one computes the mathematical distance between the time evolution sequence of the initial state of the system φ_0 and any fixed state $v \neq \varphi_0$ in the same Hilbert space. The time evolution of φ_0 under the action of the Hamiltonian $H_{s,\varepsilon}$ is given by the sequence $\{\varphi_0, H_{s,\varepsilon} \varphi_0, H_{s,\varepsilon}^2 \varphi_0, \dots, H_{s,\varepsilon}^\tau \varphi_0\}$, where $\tau \in \mathbb{N}$ is the number of timesteps. For a nontrivial vector $v \neq \varphi_0$, we define the distance parameter (mathematical distance) as

$$D_{s,\varepsilon}^\tau := \sqrt{1 - \sum_{k=0}^{\tau} \left(\frac{\langle v, \varphi_k' \rangle}{\|v\| \|\varphi_k'\|} \right)^2}, \quad (5)$$

where $\{\varphi'_0, \varphi'_1, \varphi'_2, \dots, \varphi'_\tau\}$ is the sequence of $\ell^2(\mathbb{Z})$ vectors obtained from Gram-Schmidt orthogonalization¹ of the sequence $\{\varphi_0, H_{s,\epsilon}\varphi_0, H_{s,\epsilon}^2\varphi_0, \dots, H_{s,\epsilon}^\tau\varphi_0\}$. Here, $\langle \cdot, \cdot \rangle$ is the $\ell^2(\mathbb{Z})$ inner product and $\|\cdot\|$ denotes the norm in the Hilbert space. Liaw [19] used results from spectral theory to numerically verify the following extended states conjecture:

For an Anderson-type Hamiltonian H , if one can find a nontrivial vector v , for which the limit of the distance parameter D approaches a positive value as time approaches infinity, then the spectrum of H includes an absolutely continuous part², which indicates the existence of extended energy states.

In other words, if one demonstrates with positive probability that

$$\lim_{\tau \rightarrow \infty} D_{s,\epsilon}^\tau > 0, \quad (6)$$

then the time-evolved transport behavior of the system under the action of the examined Hamiltonian exhibits de-localization at some energies. This spectral analysis was previously used to numerically demonstrate the existence of extended states in two-dimensional lattices of various geometries at small disorder in the nearest-neighbor (local) approximation [44]–[47]. Here we use the spectral method to investigate how the transport behavior in 1D media with random disorder is affected by nonlocal interactions. The specific problem of photon transport through a semi-crystalline polymer is considered due to the discrete nature of photon interactions and the complexity of the polymer medium.

III. LIGHT TRANSPORT THROUGH A SEMI-CRYSTALLINE POLYMER

A fundamental topic in the study of both artificial polymers and biopolymers is understanding how the molecular structure and orientations of polymer chains determine the macroscopic properties of the material. The molecular orientation within a polymer sample can be determined by measuring its birefringence properties. Birefringence is a phenomenon where an incident light beam is split into two mutually orthogonal rays, called ordinary ray and extraordinary ray (Fig. 2a), which travel with different velocities inside the birefringent material. The ordinary ray travels through the material with the same velocity in every direction, as it would have traveled in an isotropic crystal, while the extraordinary ray travels with a velocity dependent on the propagation direction within the crystal. Birefringent spectroscopy (Section 2.5.4 of [48]) is an optical technique in which the sum of the polarizability of all molecular chains within the polymer yields a measurable retardation between the ordinary and extraordinary rays produced by light transmission through a sample material. Here we provide a physical interpretation of equation (5) in the context of such retardation between orthogonal components.

¹ Note that a Gram-Schmidt orthogonalization is employed for the proper definition of a mathematical distance in the τ -dimensional Hilbert space.

² The spectrum of a Hamiltonian H consists of: (i) an absolutely continuous part, corresponding to extended states and (ii) a singular part, which includes discrete eigenvalues and poorly behaved transitional states (called singular-continuous part of the spectrum). If the spectrum of H coincides with the singular part (i), transport in the examined problem is localized. In the presence of non-vanishing absolutely continuous part of the spectrum, de-localization occurs in the form of extended states (by the RAGE theorem, see e.g., Section 1.2 of [43]).

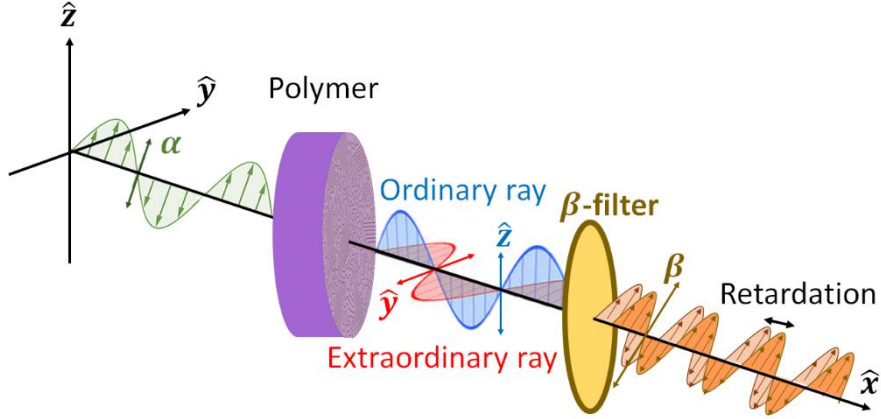


Figure 2. Birefringent spectroscopy: Light, initially polarized at an angle α_0 is transmitted through a polymer sample with birefringent properties. The resulting ordinary and extraordinary rays are then passed through an analyzer filter with a fixed polarization $\beta \neq \alpha_0$, which yields a measurable retardation between the two rays.

As semi-crystalline polymers are characterized both by disorder and nonlocal interactions [22], [23], the operator in (1) is appropriate for describing the Hamiltonian structure of such materials. Light transport in disordered media is characterized by a multiple-scattering process resulting from random fluctuations of the refractive index in space [49]. The addition of non-local interactions can result in anomalous diffusion of light, which has been experimentally observed in heterogeneous dielectric materials [50] and in hot atomic vapors [51]. Although polymers are often highly disordered, network-mediated non-local interactions can naturally arise from the intricate folding of their molecular chains (e.g., protein folding [52]) or can be artificially induced by doping (e.g., organic semiconductors [53]). Figure 3a shows a schematic representation of a semi-crystalline polymer structure, which exhibits both disorder and crystalline regions of characteristic scale.

Here we consider a problem, where a plane-polarized light beam is transmitted through a semi-crystalline polymer, and then passed through another polarization filter (Fig. 2). Assume that the initial polarization direction α of the beam changes due to successive interactions of the light photons with structures within the lattice. The goal is to quantify the change in light polarization and relate it to the structure of the medium. A photon-based description of this process requires discretization, such as the one provided by Dirac in Sec. 2 of [54]. Dirac proposed that light plane-polarized in a certain direction α can be described as consisting of photons, each polarized in the same direction α . Using a simple example ³, Dirac argued that when α -polarized light passes through β -oriented single slit, the probability of a photon being transmitted approaches $\sin^2 \alpha$, while the probability of a photon being blocked approaches $\cos^2 \alpha$. Conservation of probability is now ensured by the relation $1 = \sin^2 \alpha + \cos^2 \alpha$. These probabilities coincide with the experimentally measurable fractions of transmitted and blocked light, which justifies the discretized representation.

Similarly, we generalize Dirac's representation to the problem where the α -polarized light photons interact with the complex structure of the polymer, instead of a simple slit, and are then transmitted

³ An expanded discussion of the Dirac example can be found in Appendix A.

through a β -polarized filter. The question of interest is how photon interactions with the complex molecular structures within the sample affects the probability of light retardation, measurable by the analyzer filter. In the following, we obtain the time evolution of photon polarization direction due to successive interactions within the polymer sample by iterative application of the operator in equation (1) to the initial polarization state ⁴. In this representation, we show that the distance parameter $D_{s,\epsilon}^\tau$ in equation (5) can be used to quantify the probability that a photon is transmitted along an optical axis, defined by the crystalline structures within the amorphous medium.

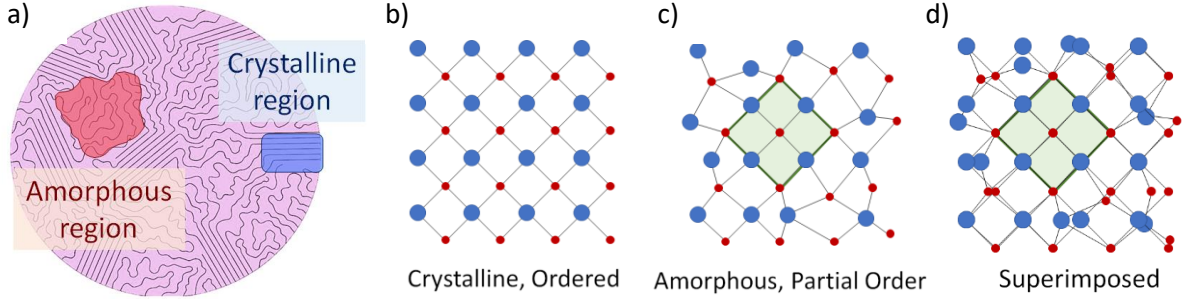


Figure 3. a) Schematic representation of semi-crystalline polymer showing regions of ordered and disordered structures, consisting of folded molecular chains. b) Crystalline and c) partially ordered amorphous structures can be d) superimposed to determine the scale of crystalline regions. The distance parameter in equation (5) can be used to quantify the scale of crystalline regions within the semi-crystalline sample.

Specifically, consider the 1D Hilbert space \mathcal{H} whose basis vectors δ_i represent the lattice points along the direction of light propagation where the light beam interacts with the sample molecules. The Hamiltonian structure of the polymer sample is modeled by the operator $H_{s,\epsilon}$ in equation (2), where the random disorder term corresponds to stochastic fluctuations $\{\epsilon_i\}$ in the polarizability of molecular bonds (e.g., due to spatial defects), while the fractional Laplacian accounts for nonlocal scattering events (e.g., due to folding of the molecular chains, as shown in Fig. 3a). Following the photon description by Dirac, let the incident light beam consist of photons, each polarized in the same direction. Denote this initial state by the vector δ_0 and assign to this state the value 1. This represents a plane-polarized light beam that enters the sample at an initial contact point δ_0 . The iterative application of $H_{s,\epsilon}$ on the initial state δ_0 yields the time evolution of photon polarization, given by the sequence $\{\delta_0, H_{s,\epsilon}\delta_0, H_{s,\epsilon}^2\delta_0, \dots, H_{s,\epsilon}^\tau\delta_0\}$, where τ is the number of timesteps. Using the Gram-Schmidt procedure, one can orthogonalize the members of this sequence to obtain the sequence $\{\phi'_0, \phi'_1, \phi'_2, \dots, \phi'_\tau\}$, which now quantifies the accumulation of *new* polarization information as the light beam propagates to new contact points δ_i after each scattering event

Assume that the semi-crystalline polymer sample contains regions of ordered structures, which behave like uniaxial crystals (Fig. 3a) of characteristic scale. To model such regions, consider a vector of the form

$$\hat{v} = \frac{v}{\|v\|} = \frac{1}{L} \sum_{j=1}^L \delta_j, \quad (7)$$

⁴ The use of unitary and Hermitian operators that evolve the polarization state of photons in time is common in the study of birefringent crystals [55].

which is a linear combination of L number of basis vectors in the Hilbert space, with equal weights. This vector corresponds to a perfectly ordered 1D lattice with L distinct contact points and can be used as a test lattice reflecting the expected scale of crystalline regions within the semi-crystalline polymer (Fig. 3b, c, d). After each interaction event (application of $H_{s,\epsilon}$), the photon changes polarization in such a way that allows it to travel either along the optic axis of the crystalline structure or in a direction orthogonal to it, with a certain probability. Substituting expression (7) into equation (5) gives

$$D_{s,\epsilon}^\tau := \sqrt{1 - \sum_{k=0}^{\tau} \left(\frac{\langle v, \varphi'_k \rangle}{\|v\| \|\varphi'_k\|} \right)^2} = \sqrt{1 - \sum_{k=0}^{\tau} \cos^2 \alpha_k}, \quad (8)$$

where α_k is the generalized angle between the vector direction \hat{v} and the new polarization direction, generated at the k th timestep of the iteration process. Due to the Gram-Schmidt orthogonalization used to obtain the sequence $\{\varphi'_0, \varphi'_1, \varphi'_2, \dots, \varphi'_\tau\}$ and the normalization in equations (7) and (8), at each timestep, the component $\cos^2 \alpha_k$ and the component $D_{s,\epsilon}^k$ are orthogonal. Thus, in this representation, the distance parameter has the same function as $\sin^2 \alpha$ in the Dirac example, which allows for a similar interpretation. For a large number of scattering events (large τ), $\sum_{k=0}^{\tau} \cos^2 \alpha_k$ represents the probability that the photon belongs to an ordinary light ray that propagates in a perfectly ordered crystalline region of fixed finite size L , while $(D_{s,\epsilon}^\tau)^2 = 1 - \sum_{k=0}^{\tau} \cos^2 \alpha_k$ quantifies the probability that new scattering information is generated due to the dissimilarity between the idealized reference lattice and the examined polymer structure. The conservation of probability in this case is ensured by the Pythagorean Theorem in the Hilbert space.

In other words, the plot $D_{s,\epsilon}^\tau(\tau)$ provides a measure of the difference between polarization directions accumulated under the action of the Hamiltonian $H_{s,\epsilon}$ and the polarization direction defined by a perfectly-ordered crystalline region of characteristic scale L . Therefore, by varying the number L of polarization directions δ_j in the reference lattice and/or the weights for each δ_j (fluctuations in the atomic order), one can examine the characteristics of polarization information generated by the iterations of the Hamiltonian. If the successive iterations continue to generate new polarization directions as $\tau \rightarrow \infty$, the difference component $D_{s,\epsilon}^\tau$ is nonvanishing with respect to the reference lattice, indicating dissimilarity between the assumed size/order of crystalline regions and the actual structure of the sample.

As discussed in Sec. II, $\lim_{\tau \rightarrow \infty} D_{s,\epsilon}^\tau > 0$ indicates the existence of extended states, or transport. Thus, in the present representation, a nonvanishing limiting value of the distance parameter suggests transport beyond the chosen reference lattice scale. In contrast, if $\lim_{\tau \rightarrow \infty} D_{s,\epsilon}^\tau = 0$ for a certain choice of the reference lattice \hat{v} , the structure of the sample is expected to exhibit regions of crystallinity characterized by size/order, comparable to \hat{v} . Section IV presents a numerical study of transport through semi-crystalline polymer structure described by the Hamiltonian in equation (1). In this study, we fix the weights on the reference lattice vector and vary its size for different choices of disorder concentration and properties of the fractional Laplacian. The application of equation (5) when the calculation is performed using a reference lattice with randomly selected vector weights will be explored in our future work.

IV. RESULTS AND DISCUSSION

In this section, we conduct a numerical experiment where the distance parameter in equation (5) is computed for various choices of disorder concentration c , type of nonlocal interactions (characterized by s), and scale of a reference lattice vector \hat{v} . Each plot $D_{s,\epsilon}^{\tau}(\tau)$ is an average of at least 10 realizations for the selected parameters, which minimizes inaccuracies due to the random realization of disorder values. All numerical experiments are calculated for $\tau = 10,000$ timesteps, which corresponds to $N = 20,001$ lattice sites in 1D-space. The semi-crystalline polymer structure is modeled by the Hamiltonian in equation (2), with a discrete fractional Laplacian from equations (4) and (5). Throughout this study, the concentration of disorder c is allowed to vary in magnitude, but in all numerical experiments, the random disorder values $\epsilon_i \in [-c/2, c/2]$ are selected according to a uniform (flat) distribution. (See Kostadinova, et al. [44] for a study of transport in a 2D lattice, where disorder is selected from a Gaussian and a modified Gaussian distribution.) To model the different diffusion regimes resulting from nonlocal interactions, one can vary the fraction on the Laplacian in the interval $s \in (0,1)$ for super-diffusion, $s \in (1,2)$ for sub-diffusion, or fix it to $s = 1$ for normal (Fickian) diffusion. The present study is focused on three choices $s = 0.9, 1, 1.1$, which are considered representative for each regime. Once the distribution of disorder and fraction on the Laplacian are fixed, we vary the size L of a reference lattice vector, which is set by the number of terms in the summation of equation (7).

While the classical Laplacian Δ models nearest-neighbor (local) interactions, the application of a fractional Laplacian $(-\Delta)^s$ results in interactions that, in principle, extend to infinity. In other words, the analytical expression in equation (3) is exact when the summation is performed over infinite number of nearest neighbors at each timestep. Due to the finite nature of the numerical simulation, we restrict the calculation to a finite number of nearest neighbors, which we call the *range* of nonlocal interactions, which sets the upper limit for the summation in equation (3). Introducing such cutoff is not entirely unphysical since nonlocal forces in nature can also exhibit characteristic scales at which resulting interactions are appreciable (for example, consider shielding lengths in plasmas). Appendix B provides further discussion on the choice of truncation and its possible effect on numerical results.

Initially, we examine cases where the reference vector size is the same as the assumed range of nonlocal interactions, i.e., $L \equiv \text{range}$. This intuitive choice makes sense when one considers the folded chains forming the semi-crystalline polymer structure in Fig. 3a and the simplified picture in Fig. 4. Although any fold of a molecular chain yields the possibility of non-local transport through network-mediated interactions, the increased complexity of folds in the amorphous regions can result in transport retardation (or sub-diffusion). In contrast, a symmetric fold within the crystalline regions can enhance transport, with increasing possibility of super-diffusion when the molecular chain is stretched. Thus, it is reasonable to expect that a correspondence exists between the characteristic size of the crystalline region and the average range of nonlocal effects, mediated by the molecular chain structure and length. The degree of crystallinity as a function of time has been studied for various molecular weights (number of molecules per chain) in polymers. It has been established that for many types of polymers, higher

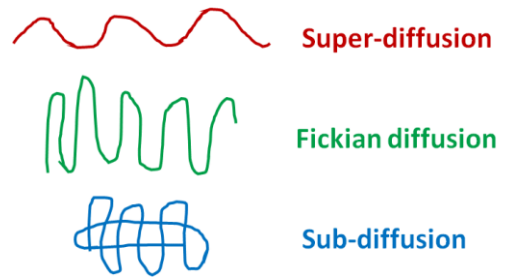


Fig. 4. Visual representation of the relation between molecular chain fold and diffusion regime.

molecular weight reduces the degree of crystallinity and increases the thickness of the amorphous region [56]–[59]. Due to the existence of such a relation, our initial assumption is that the size of the reference vector L in our model should be comparable to the range of non-local interactions $range$, which corresponds to the size of the crystalline region. However, in complex materials, such as polymers, the presence of random disorder further complicates such relation. Therefore, in the following analysis, we consider both cases where $range = L$ and where $range \neq L$.

To examine the dependence on disorder concentration c in the three diffusion regimes, we initially fix the range of nonlocal interactions to $range = 300$ and consider only a reference vector of the same size $L = 300$. Figure 5 shows the time evolution of distance parameters, where the disorder concentration c is varied across four scales from $c \sim 10^{-4}$ to $c \sim 10^{-1}$. In each plot, white dashed lines are used to distinguish among the four disorder regions. For the smallest examined disorder interval, $c \sim 10^{-4}$, the value of $D_{s,\epsilon}^r$ does not decrease appreciably from 1 in the super-diffusive regime (Fig. 5a), while substantial decrease is observed for the sub-diffusive case (Fig. 5c). The classical diffusion case shows a small decrease in $D_{s,\epsilon}^r$ for $c \sim 10^{-4}$, which is clearly enhanced in the range where $c \sim 10^{-3}$ (Fig. 5b). For all three diffusion regimes, the distance values drop rapidly to zero for the higher disorder ranges of $c \sim 10^{-2}$ and $c \sim 10^{-1}$, while preserving the expected overall behavior (i.e., sub-diffusive case decreases slower than diffusive, which decreases slower than super-diffusive).

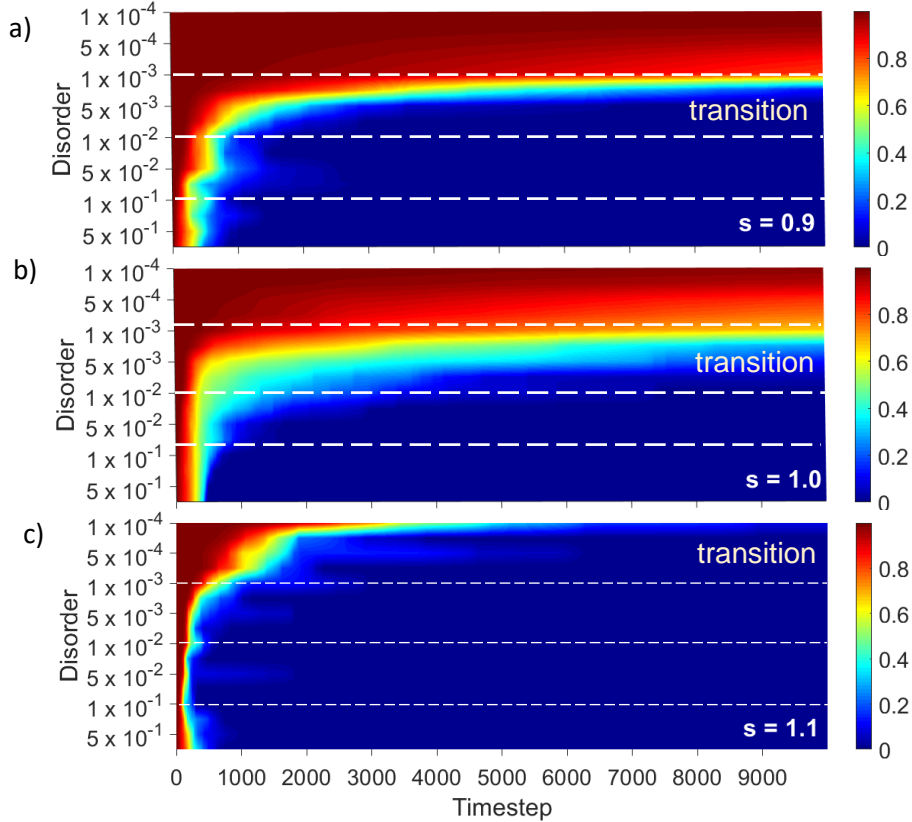


Fig. 5. Time evolution of distance parameter for various choices of disorder concentration in the a) super-diffusive, b) diffusive, and c) sub-diffusive regime. The color bar indicates the value of the computed distance value. In each plot, the dashed lines identify the four examined disorder scales.

The regions where the distance plots transition from slow decrease (de-localized behavior) to rapid drops are clearly visible in Fig. 5. The range $c \sim 10^{-3}$ seems transitional for both super-diffusive and diffusive realizations, while the sub-diffusive case exhibits greatest variation of distance values only for the smallest values of disorder in the range $c \sim 10^{-4}$. Figure 6 shows time evolution of distance plots for representative values from these two disorder scales. In the smaller range of disorder, where $c \sim 10^{-4}$, for all examined cases the super-diffusive realizations decrease slower with time than the diffusive, which in turn decrease slower than the sub-diffusive ones, which we call the expected behavior (Fig. 6a). For values $c > 1 \times 10^{-3}$, we observe deviations from the expected behavior, in which both super- and sub-diffusive realizations decrease faster than the classical diffusion case (Fig. 6b). Since transport in a one-dimensional lattice is highly sensitive to concentration of disorder, higher concentrations lead to localization of all transport, even in the presence of long-distance positive correlations. In this case, the possibility for nonlocal interaction in the anomalous diffusion realizations does not produce qualitatively different transport behavior; instead, it allows the system to reach localization more rapidly. Since we are interested in regimes where different diffusion is observable, the following analysis is focused on cases where $c \leq 1 \times 10^{-3}$.

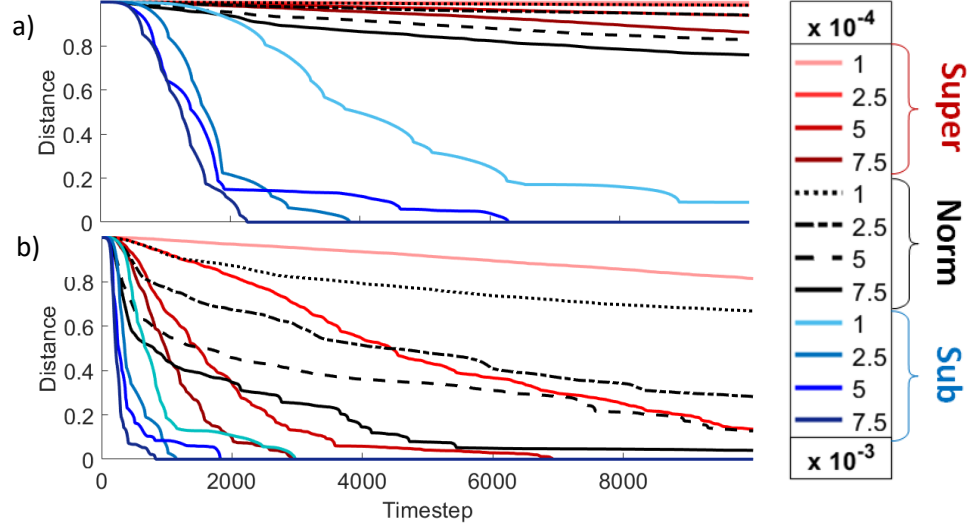


Fig. 6. Time evolution of distance parameter for super diffusion (red shades), normal diffusion (black), and sub-diffusion (blue shades) in the disorder range where a) $c \sim 10^{-4}$ and b) $c \sim 10^{-3}$.

To determine the expected size of crystalline regions in the semi-crystalline polymer, we fixed the concentration of disorder to $c = 1 \times 10^{-3}$ and examined how the distance plots change as a function of a reference lattice scale L in the three diffusion regimes. As discussed in Sec. III, the physical interpretation of positive limiting value of $D_{s,\epsilon}^\tau$ as $\tau \rightarrow \infty$ is the existence of extended states, or transport, in a region of size comparable to the selected reference lattice vector size L . In other words, for a given choice of a Hamiltonian $H_{s,\epsilon}$, if $\lim_{\tau \rightarrow \infty} D_{s,\epsilon}^\tau > 0$, it is likely that transport is enhanced at the examined scale L , with the likelihood proportional to the limiting value of $D_{s,\epsilon}^\tau$. Conversely, if the distance rapidly drops to zero for a given L , it is expected that transport under the action of $H_{s,\epsilon}$ is impeded at that scale. Thus, in the following analysis, we associate slowly decreasing distance plots with possible crystalline regions and rapidly decreasing plots with unlikely scales for the development of crystalline structures.

Assuming that the range of nonlocal interactions in the sub- and super-diffusive cases is comparable to the size of crystalline regions, in Fig. 7 we show the results for the three diffusion regimes at fixed disorder $c = 1 \times 10^{-3}$ and increasing size L of the reference vector, while keeping $L = \text{range}$. The reference vector size was increased from $L = 50$ to $L = 1000$ in increments of $\Delta L = 50$. In the super-diffusive regime, the limiting $D_{s,\epsilon}^\tau$ values are positive for scales in the range $L \lesssim 450$ with a sharp transition region between nonvanishing and vanishing realizations (marked by the white dashed contour in Fig. 7a). The transition region for the classical Fickian diffusion case (white dashed contour in Fig. 7b) is much wider and smother, which is to be expected from the local (nearest neighbor) interactions used in this calculation. In other words, for a fixed number of timesteps, the distance parameter approaches its limiting behavior more slowly in the classical diffusion calculation as compared to the anomalous diffusion cases, where long-distance interactions are assumed. Nevertheless, examination of Fig. 7 clearly shows that the assumed simulation size of $\tau = 10,000$ timesteps is large enough to reveal the expected differences in the transport behavior for the three regimes. Specifically, the transition region in the classical diffusion case is much broader and shifted to include smaller scales in the range $150 \leq L \leq 400$, where the limiting distance values decrease more rapidly as compared to the same scales in the super-diffusive case. Fig. 7c indicates that, for the selected conditions, transport is suppressed at all scales, which is expected for sub-diffusive behavior.

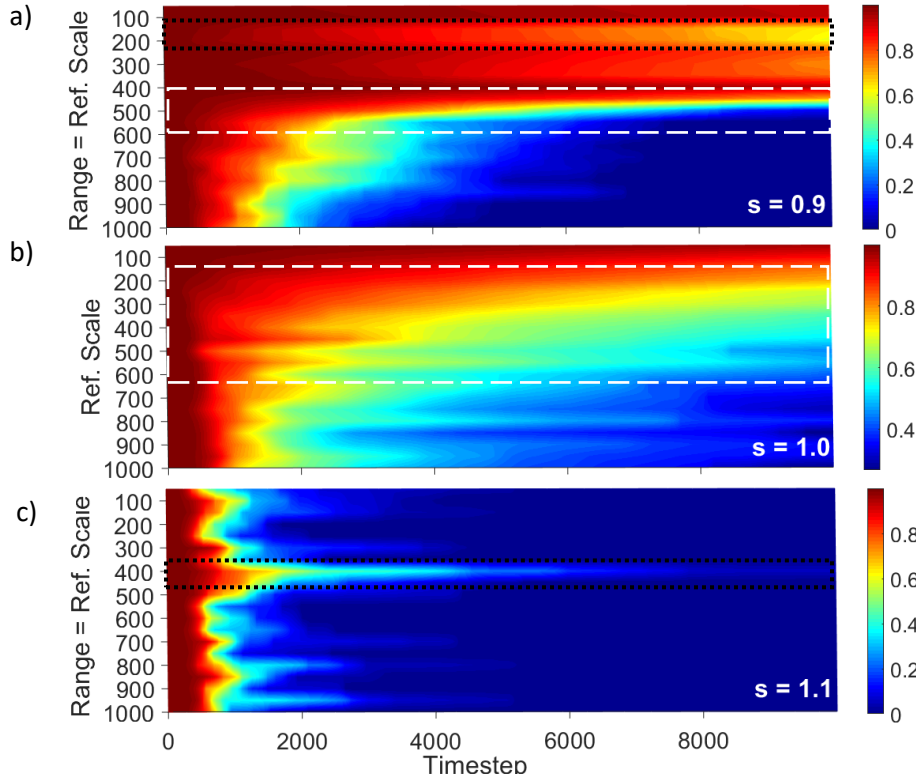


Fig. 7. Time evolution of distance parameter as a function of reference lattice scale in the a) super-diffusive, b) diffusive, and c) sub-diffusive regime. All calculations are performed for disorder $c = 1 \times 10^{-3}$ and assuming the range of non-local interactions is equal to the reference vector size. Regions where the distance plots transition from positive to vanishing limiting values are marked by a white dashed contour. Black dotted contours mark regions, where the transport seems to deviate from the expected overall behavior.

Figure 7 also shows that both anomalous diffusion regimes exhibit realizations where transport seems to deviate from the overall behavior observed at the surrounding scales. Those realizations are marked by dotted black contours in Fig. 7 and correspond to $range = L = [150, 200]$ in the super-diffusive case and $range = L \sim 400$ in the sub-diffusive case. For each set of conditions, the time evolution of the distance parameter plotted in Fig. 7 is an average of 10 realizations, which minimizes fluctuations due to the random distribution of disorder. Thus, the observed unusual realizations may represent physically observable effects, resulting from the nonlocal character of the interactions. Possible numerical instabilities due to randomness of the disorder and numerical round-off errors are further discussed in Appendix B.

To explore the interplay between range of nonlocality and reference scale, we performed numerical experiments where $range$ is varied, while keeping the reference scale fixed at $L = 300$ and the disorder fixed at $c = 1 \times 10^{-3}$. The question of interest in such experiments is how the cutoff of nonlocality affects transport at a fixed scale of interest. Figure 8 shows the results for both anomalous diffusion cases, where the nonlocality influence was increased from $range = 50$ to $range = 1000$ in increments of $\Delta range = 50$. In both regimes, the realizations corresponding to unusual transport behavior are enhanced, as shown by the black dotted contours in Fig. 8. In addition, in the super-diffusive case (Fig. 8a), transport is impeded for $range = 50$, while in the super-diffusive case (Fig. 8b), transport is enhanced for $range = 50, 100, \& 150$. For both anomalous diffusion regimes, characteristic features of the results for larger range values are mostly unaffected as compared to the plots from Fig. 7. Additionally, the transition region in the super-diffusive case (white dashed contour in Fig. 8a) is preserved. This implies that, for fixed disorder concentration and fixed scale of interest L , the transport behavior can vary significantly for a range of nonlocal interactions $range \lesssim L$ that are smaller or comparable to the examined scale. However, as the nonlocality range exceeds the spatial scale $range > L$, transport is determined solely by the type of nonlocal interactions (super- or sub-diffusive).

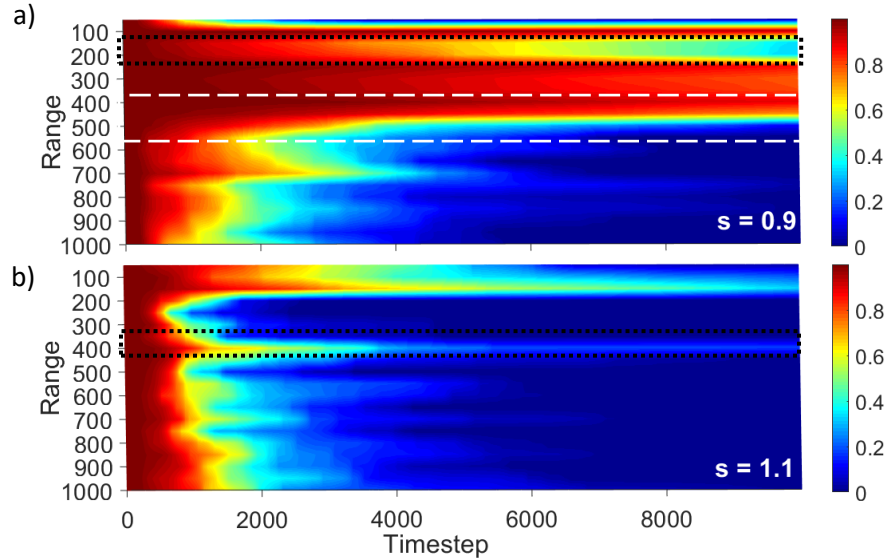


Fig. 8. Time evolution of the distance parameter for increasing range in the a) super-diffusive and b) sub-diffusive regimes. All calculations are performed for disorder $c = 1 \times 10^{-3}$ and assuming a fixed reference vector size $L = 300$. Transition regions are marked by a white dashed contour. Black dotted contours mark regions where the transport seems to deviate from the expected overall behavior.

To further examine these conclusions, we performed numerical experiments where the reference vector scale is varied, while keeping the range of nonlocal interactions fixed at $range = 300$ and the disorder fixed at $c = 1 \times 10^{-3}$. Here, the question of interest is how a given (known) range of nonlocal interactions affects transport at different spatial scales. Figure 9 shows the results for both anomalous diffusion cases, where the reference scale was increased from $L = 50$ to $L = 1000$ in increments of $\Delta L = 50$. For scales $L < 500$, which are comparable or smaller than the fixed influence $range = 300$, transport is enhanced in the super-diffusive case (Fig. 9a) and suppressed in the sub-diffusive case (Fig. 9b). As the reference scale increases, the transport behavior exhibits fluctuations, especially visible in the range $500 < L < 800$ for the sub-diffusive realizations. This result is highly unexpected since it implies that extended states can exist in a disordered system, where negative nonlocal correlations induce nonlinear diffusion.

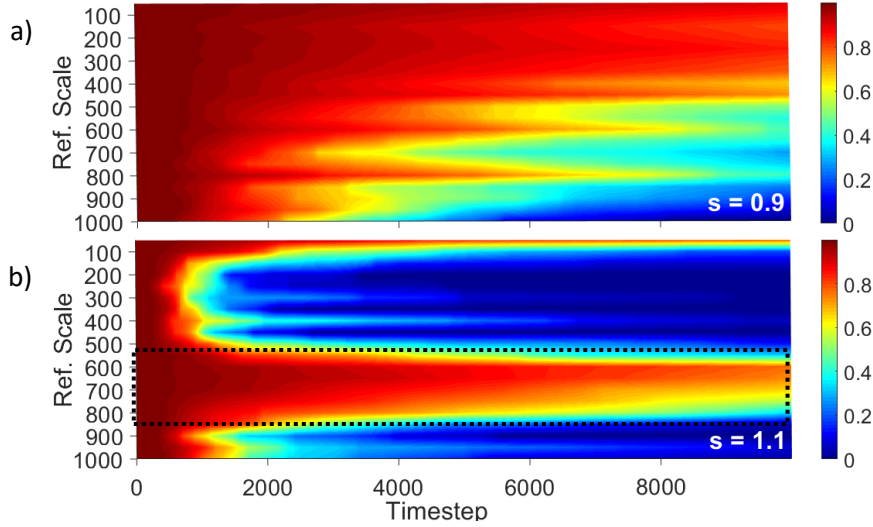


Fig. 9. Time evolution of the distance parameter for increasing reference vector scales in the a) super-diffusive and b) sub-diffusive regimes. All calculations are performed for disorder $c = 1 \times 10^{-3}$ and assuming a fixed range of nonlocal interactions $range = 300$. Black dotted contours mark the region, where the transport seems to deviate from the expected overall behavior.

A possible physical explanation for the enhanced transport observed in Fig. 9b is the interplay between the two distinct localization mechanisms acting in this case: random disorder and negative correlations. In our model, negative correlations are represented by the fractional Laplacian $(-\Delta)^s$, with exponents in the range $s \in (1,2)$, which yields nonlinear (sub-diffusive) transport. Numerical and experimental studies of one-dimensional granular crystals have recently demonstrated that disorder and nonlocality, which individually favor localization, can cancel each other and yield super-diffusive transport in the system [34], [37]. Based on examination of the various possible sources of numerical errors affecting the computation (discussed in Appendix B), we conclude that the results observed in Fig. 9b are likely to have physical significance.

Initial insight into the mechanisms guiding transport in the sub-diffusion regime can be obtained by examination of Fig. 1. The representative trajectories in Fig. 1c are overall more localized than the trajectories in the classical diffusion case (Fig. 1a) but can still exhibit big jumps due to the nonlocal interactions assumed. This implies the possibility of de-localization if the characteristic scale of these jumps is larger than the characteristic localization length due to the disorder concentration. Although the data in Fig. 1 was artificially generated for representation purposes, the mixed PDF used to obtain the trajectories in Fig. 1c was selected to reflect the physical

interpretation of the sub-diffusive fractional Laplacian, as discussed in Sec. 2, Theorem 2 of [20]. There, it was argued that in the case $s \in (1,2)$, one can write $s = 1 + \tilde{s}$, where $\tilde{s} \in (0,1)$ and the sub-diffusive operator can be decomposed into $(-\Delta)^s = (-\Delta)^{\tilde{s}}(-\Delta)$. In other words, mathematically, sub-diffusion can be considered as a superposition of two actions (classical diffusion and super-diffusion). When those two actions are composed together, there is a possibility of a “backward” movement of the particle, enhancing the probability for localization. Nevertheless, the sub-diffusive operator is still nonlocal, which allows for the presence of long-distance effects.

To reflect this logic, the trajectories in Fig. 1c were produced using a superposition of truncated Gaussian PDF (centered at the origin) and two truncated Lévy distributions (centered symmetrically with respect to the Gaussian). As can be seen in Fig. 1d, the resulting mixed PDF exhibits fast decreasing “skinny” tails and two symmetric peaks around the Gaussian. This choice of PDF results for overall enhanced localization of the trajectories but accounts for the possibility of long jumps proportional to the location of the Lévy distribution peaks. The addition of random disorder introduces fluctuations of the particle displacements, which may alter slightly the corresponding PDFs. As localization lengths decrease with increasing disorder, there is a characteristic scale defined by this type of localization process. Thus, we expect that de-localization can be achieved in the sub-diffusion regime if the scale of the long-distance jumps allowed in this regime exceeds the expected localization scales for a given disorder.

V. CONCLUSIONS AND FUTURE WORK

Here we presented a numerical study of transport in disordered media, where nonlocal interactions may arise due to positive or negative correlations. The numerical experiments were performed using a Fractional Laplacian Spectral (FLS) model, which combines the spectral approach to the Anderson localization problem [19] with a series representation of the fractional Laplacian [20]. The resulting code models transport guided both by interactions with random potentials and by nonlocal effects resulting in nonlinear (anomalous) diffusion. We developed a physical interpretation of the FLS model adapted for the study of light diffusion through a semi-crystalline polymer structure. A major finding of the numerical experiments is an unexpected transport enhancement at key spatial scales resulting from the interplay between competing localization effects. The existence of this effect has been recently discovered in experiments with 1D granular chains [34]. As polymers consist of large molecular chains, the presence of such anomalous transport may be related to key properties of the polymer structure, such as the formation of crystalline or amorphous regions resulting from particular folding sequences of the molecular chains. Thus, we expect that the findings of the present study can be extended and adapted to specific problems of interest within the greater science community, including research in electrorheological fluids, organic semi-conductors, proteins, and DNA.

Of specific interest to our future work is testing the predictions of the FLS models using numerical and laboratory experiments with multi-chain dusty plasmas. These are arrangements of charged grains into string-like structures, which can be thought of as macroscopic analogues to molecular chains in polymers. The field of complex (or dusty) plasmas investigates the dynamics of mesoscopic particles (or dust) suspended in weakly-ionized low temperature plasma. Dust grains immersed in plasma become negatively charged and are subject to both ion drag forces and collective (nonlocal) interactions. As a result, dusty plasmas can self-organize into strongly

coupled fluids with electrorheological properties, i.e., the ability to undergo homogeneous-to-string structural transitions when acted upon with electric fields [60], [61]. More importantly, the dust particles are directly observable with a video camera, which makes them ideal for the study of self-organization and stability, phase transitions, and transport phenomena at the kinetic (individual-particle) level. This allows for the direct examination of anomalous diffusion as a function of scale and range of nonlocal interactions. The former is defined by the number of particles forming chains in the dusty plasma liquid, while the latter can be varied by tuning the plasma parameters in the experiment.

ACKNOWLEDGMENTS

This work was supported by the NSF grant numbers 1903450 (EGK, JLP, CDL, and LSM), 1707215 (LSM and TWH), and 1740203 (TWH and LSM), NSF-DMS grant number 1802682 (CDL), and NASA grant number 1571701 (TWH and LSM).

BIBLIOGRAPHY

- [1] K. Pearson, “The Problem of the Random Walk,” *Nature*, vol. 72, no. 1865, pp. 294–294, Jul. 1905, doi: 10.1038/072294b0.
- [2] A. Fick, “Ueber Diffusion,” *Ann. Phys.*, vol. 170, no. 1, pp. 59–86, 1855, doi: 10.1002/andp.18551700105.
- [3] A. Einstein, *Investigations on the Theory of the Brownian Movement*. Courier Corporation, 1956.
- [4] N. Tarantino *et al.*, “TNF and IL-1 exhibit distinct ubiquitin requirements for inducing NEMO–IKK supramolecular structures,” *J. Cell Biol.*, vol. 204, no. 2, pp. 231–245, Jan. 2014, doi: 10.1083/jcb.201307172.
- [5] J. Klafter and I. M. Sokolov, “Anomalous diffusion spreads its wings,” *Phys. World*, vol. 18, no. 8, pp. 29–32, Aug. 2005, doi: 10.1088/2058-7058/18/8/33.
- [6] G. M. Viswanathan, V. Afanasyev, S. V. Buldyrev, E. J. Murphy, P. A. Prince, and H. E. Stanley, “Lévy flight search patterns of wandering albatrosses,” *Nature*, vol. 381, no. 6581, pp. 413–415, May 1996, doi: 10.1038/381413a0.
- [7] R. P. D. Atkinson, C. J. Rhodes, D. W. Macdonald, and R. M. Anderson, “Scale-free dynamics in the movement patterns of jackals,” *Oikos*, vol. 98, no. 1, pp. 134–140, 2002, doi: 10.1034/j.1600-0706.2002.980114.x.
- [8] G. Ramos-Fernández, J. L. Mateos, O. Miramontes, G. Cocho, H. Larralde, and B. Ayala-Orozco, “Lévy walk patterns in the foraging movements of spider monkeys (*Ateles geoffroyi*),” *Behav. Ecol. Sociobiol.*, vol. 55, no. 3, pp. 223–230, Jan. 2004, doi: 10.1007/s00265-003-0700-6.
- [9] Y. Zhang *et al.*, “Identification of Pollutant Source for Super-Diffusion in Aquifers and Rivers with Bounded Domains,” *Water Resour. Res.*, vol. 54, no. 9, pp. 7092–7108, 2018, doi: 10.1029/2018WR023011.
- [10] Y. Zhang, M. M. Meerschaert, and R. M. Neupauer, “Backward fractional advection dispersion model for contaminant source prediction,” *Water Resour. Res.*, vol. 52, no. 4, pp. 2462–2473, 2016, doi: 10.1002/2015WR018515.
- [11] A. Shalchi, “Magnetic Field Line Random Walk in Two-dimensional Turbulence: Markovian Diffusion versus Superdiffusion,” *Contrib. Plasma Phys.*, vol. 51, no. 10, pp. 920–930, 2011, doi: 10.1002/ctpp.201100106.
- [12] D. del-Castillo-Negrete, B. A. Carreras, and V. E. Lynch, “Nondiffusive Transport in Plasma Turbulence: A Fractional Diffusion Approach,” *Phys. Rev. Lett.*, vol. 94, no. 6, p. 065003, Feb. 2005, doi: 10.1103/PhysRevLett.94.065003.

- [13] K. W. Gentle *et al.*, “An experimental counter-example to the local transport paradigm,” *Phys. Plasmas*, vol. 2, no. 6, pp. 2292–2298, Jun. 1995, doi: 10.1063/1.871252.
- [14] H. Scher and E. W. Montroll, “Anomalous transit-time dispersion in amorphous solids,” *Phys. Rev. B*, vol. 12, no. 6, pp. 2455–2477, Sep. 1975, doi: 10.1103/PhysRevB.12.2455.
- [15] J. Kang, F. Zhou, T. Xia, and G. Ye, “Numerical modeling and experimental validation of anomalous time and space subdiffusion for gas transport in porous coal matrix,” *Int. J. Heat Mass Transf.*, vol. 100, pp. 747–757, Sep. 2016, doi: 10.1016/j.ijheatmasstransfer.2016.04.110.
- [16] K. Ritchie, X.-Y. Shan, J. Kondo, K. Iwasawa, T. Fujiwara, and A. Kusumi, “Detection of Non-Brownian Diffusion in the Cell Membrane in Single Molecule Tracking,” *Biophys. J.*, vol. 88, no. 3, pp. 2266–2277, Mar. 2005, doi: 10.1529/biophysj.104.054106.
- [17] T. K. Fujiwara *et al.*, “Confined diffusion of transmembrane proteins and lipids induced by the same actin meshwork lining the plasma membrane,” *Mol. Biol. Cell*, vol. 27, no. 7, pp. 1101–1119, Feb. 2016, doi: 10.1091/mbc.E15-04-0186.
- [18] W. Min, G. Luo, B. J. Cherayil, S. C. Kou, and X. S. Xie, “Observation of a Power-Law Memory Kernel for Fluctuations within a Single Protein Molecule,” *Phys. Rev. Lett.*, vol. 94, no. 19, p. 198302, May 2005, doi: 10.1103/PhysRevLett.94.198302.
- [19] C. Liaw, “Approach to the Extended States Conjecture,” *J Stat Phys*, vol. 153, pp. 1022–1038, Nov. 2013, doi: 10.1007/s10955-013-0879-5.
- [20] J. L. Padgett, E. G. Kostadinova, C. D. Liaw, K. Busse, L. S. Matthews, and T. W. Hyde, “Anomalous diffusion in one-dimensional disordered systems: a discrete fractional Laplacian method,” *J. Phys. Math. Theor.*, vol. 53, no. 13, p. 135205, Mar. 2020, doi: 10.1088/1751-8121/ab7499.
- [21] V. Jakšić and Y. Last, “Simplicity of singular spectrum in Anderson-type Hamiltonians,” *Duke Math. J.*, vol. 133, no. 1, pp. 185–204, May 2006, doi: 10.1215/S0012-7094-06-13316-1.
- [22] C.-C. Cheng, W.-T. Chuang, D.-J. Lee, Z. Xin, and C.-W. Chiu, “Supramolecular Polymer Network-Mediated Self-Assembly of Semicrystalline Polymers with Excellent Crystalline Performance,” *Macromol. Rapid Commun.*, vol. 38, no. 5, p. 1600702, 2017, doi: 10.1002/marc.201600702.
- [23] L. D. Michele, A. Zacccone, and E. Eiser, “Analytical theory of polymer-network-mediated interaction between colloidal particles,” *Proc. Natl. Acad. Sci.*, vol. 109, no. 26, pp. 10187–10192, Jun. 2012, doi: 10.1073/pnas.1202171109.
- [24] P. W. Anderson, “Absence of Diffusion in Certain Random Lattices,” *Phys. Rev.*, vol. 109, no. 5, Mar. 1958.
- [25] A. Gerdani *et al.*, “Experimental Investigation of Superdiffusion via Coherent Disordered Quantum Walks,” *Phys. Rev. Lett.*, vol. 123, no. 14, p. 140501, Oct. 2019, doi: 10.1103/PhysRevLett.123.140501.
- [26] S. E. Skipetrov, A. Minguzzi, B. A. van Tiggelen, and B. Shapiro, “Anderson Localization of a Bose-Einstein Condensate in a 3D Random Potential,” *Phys. Rev. Lett.*, vol. 100, no. 16, p. 165301, Apr. 2008, doi: 10.1103/PhysRevLett.100.165301.
- [27] “Anderson localization of light | Nature Photonics.”
<https://www.nature.com/articles/nphoton.2013.30> (accessed Nov. 18, 2019).
- [28] J. Billy *et al.*, “Direct observation of Anderson localization of matter waves in a controlled disorder,” *Nature*, vol. 453, no. 7197, pp. 891–894, Jun. 2008, doi: 10.1038/nature07000.
- [29] A. Kekić and R. A. Van Gorder, “Wave propagation across interfaces induced by different interaction exponents in ordered and disordered Hertz-like granular chains,” *Phys. Nonlinear Phenom.*, vol. 384–385, pp. 18–33, Dec. 2018, doi: 10.1016/j.physd.2018.07.007.
- [30] L. Fleishman and P. W. Anderson, “Interactions and the Anderson transition,” *Phys. Rev. B*, vol. 21, no. 6, pp. 2366–2377, Mar. 1980, doi: 10.1103/PhysRevB.21.2366.
- [31] V. Oganessian and D. A. Huse, “Localization of interacting fermions at high temperature,” *Phys. Rev. B*, vol. 75, no. 15, p. 155111, Apr. 2007, doi: 10.1103/PhysRevB.75.155111.

- [32] J. Z. Imbrie, “On Many-Body Localization for Quantum Spin Chains,” *J. Stat. Phys.*, vol. 163, no. 5, pp. 998–1048, Jun. 2016, doi: 10.1007/s10955-016-1508-x.
- [33] D. M. Basko, I. L. Aleiner, and B. L. Altshuler, “Metal–insulator transition in a weakly interacting many-electron system with localized single-particle states,” *Ann. Phys.*, vol. 321, no. 5, pp. 1126–1205, May 2006, doi: 10.1016/j.aop.2005.11.014.
- [34] E. Kim, A. J. Martínez, S. E. Phenisee, P. G. Kevrekidis, M. A. Porter, and J. Yang, “Direct measurement of superdiffusive energy transport in disordered granular chains,” *Nat. Commun.*, vol. 9, no. 1, pp. 1–6, Feb. 2018, doi: 10.1038/s41467-018-03015-3.
- [35] V. Folli and C. Conti, “Frustrated Brownian Motion of Nonlocal Solitary Waves,” *Phys. Rev. Lett.*, vol. 104, no. 19, p. 193901, May 2010, doi: 10.1103/PhysRevLett.104.193901.
- [36] M. Peccianti, C. Conti, G. Assanto, A. D. Luca, and C. Umeton, “Routing of anisotropic spatial solitons and modulational instability in liquid crystals,” *Nature*, vol. 432, no. 7018, pp. 733–737, Dec. 2004, doi: 10.1038/nature03101.
- [37] A. J. Martínez, P. G. Kevrekidis, and M. A. Porter, “Superdiffusive transport and energy localization in disordered granular crystals,” *Phys. Rev. E*, vol. 93, no. 2, p. 022902, Feb. 2016, doi: 10.1103/PhysRevE.93.022902.
- [38] V. V. Uchaikin, “Self-similar anomalous diffusion and Levy-stable laws,” *Phys.-Uspekhi*, vol. 46, no. 8, p. 821, 2003, doi: 10.1070/PU2003v046n08ABEH001324.
- [39] R. Metzler and J. Klafter, “The random walk’s guide to anomalous diffusion: a fractional dynamics approach,” *Phys. Rep.*, vol. 339, no. 1, pp. 1–77, Dec. 2000, doi: 10.1016/S0370-1573(00)00070-3.
- [40] M. Kwaśnicki, “Ten equivalent definitions of the fractional laplace operator,” *Fract. Calc. Appl. Anal.*, vol. 20, no. 1, pp. 7–51, 2017, doi: 10.1515/fca-2017-0002.
- [41] L. Caffarelli and L. Silvestre, “An Extension Problem Related to the Fractional Laplacian,” *Commun. Partial Differ. Equ.*, vol. 32, no. 8, pp. 1245–1260, Aug. 2007, doi: 10.1080/03605300600987306.
- [42] Y. K. Chen, Z. Lei, and C. H. Wei, “Extension Problems Related to the Higher Order Fractional Laplacian,” *Acta Math. Sin. Engl. Ser.*, vol. 34, no. 4, pp. 655–661, Apr. 2018, doi: 10.1007/s10114-017-7325-6.
- [43] D. Hundertmark, “A short introduction to Anderson localization,” in *Analysis and stochastics of growth processes and interface models*, Oxford: Oxford University Press, 2008, pp. 194–218.
- [44] E. G. Kostadinova *et al.*, “Spectral approach to transport in a two-dimensional honeycomb lattice with substitutional disorder,” *Phys. Rev. B*, vol. 99, no. 2, p. 024115, Jan. 2019, doi: 10.1103/PhysRevB.99.024115.
- [45] E. G. Kostadinova *et al.*, “Delocalization in infinite disordered two-dimensional lattices of different geometry,” *Phys. Rev. B*, vol. 96, no. 23, p. 235408, Dec. 2017, doi: 10.1103/PhysRevB.96.235408.
- [46] E. G. Kostadinova, C. D. Liaw, L. S. Matthews, and T. W. Hyde, “Physical interpretation of the spectral approach to delocalization in infinite disordered systems,” *Mater. Res. Express*, vol. 3, no. 12, p. 125904, 2016, doi: 10.1088/2053-1591/3/12/125904.
- [47] E. g. Kostadinova *et al.*, “Transport properties of disordered two-dimensional complex plasma crystal,” *Contrib. Plasma Phys.*, p. n/a-n/a, doi: 10.1002/ctpp.201700111.
- [48] J. S. Bergstrom, *Mechanics of Solid Polymers: Theory and Computational Modeling*. William Andrew, 2015.
- [49] J. Bertolotti, K. Vynck, and D. S. Wiersma, “Multiple Scattering of Light in Superdiffusive Media,” *Phys. Rev. Lett.*, vol. 105, no. 16, p. 163902, Oct. 2010, doi: 10.1103/PhysRevLett.105.163902.
- [50] P. Barthelemy, J. Bertolotti, and D. S. Wiersma, “A Lévy flight for light,” *Nature*, vol. 453, no. 7194, pp. 495–498, May 2008, doi: 10.1038/nature06948.
- [51] N. Mercadier, W. Guerin, M. Chevrollier, and R. Kaiser, “Lévy flights of photons in hot atomic vapours,” *Nat. Phys.*, vol. 5, no. 8, pp. 602–605, Aug. 2009, doi: 10.1038/nphys1286.
- [52] V. I. Abkevich, A. M. Gutin, and E. I. Shakhnovich, “Impact of Local and Non-local Interactions on Thermodynamics and Kinetics of Protein Folding,” *J. Mol. Biol.*, vol. 252, no. 4, pp. 460–471, Sep. 1995, doi: 10.1006/jmbi.1995.0511.

- [53] S.-J. Wang *et al.*, “Long spin diffusion lengths in doped conjugated polymers due to enhanced exchange coupling,” *Nat. Electron.*, vol. 2, no. 3, pp. 98–107, Mar. 2019, doi: 10.1038/s41928-019-0222-5.
- [54] P. A. M. Dirac, *The Principles of Quantum Mechanics*. Clarendon Press, 1981.
- [55] P. W. Atkins and L. D. Barron, “A polarization density matrix description of birefringent photon scattering,” *Mol. Phys.*, vol. 18, no. 6, pp. 721–727, Jun. 1970, doi: 10.1080/00268977000100781.
- [56] W. Rungswang *et al.*, “Influences of tacticity and molecular weight on crystallization kinetic and crystal morphology under isothermal crystallization: Evidence of tapering in lamellar width,” *Polymer*, vol. 172, pp. 41–51, May 2019, doi: 10.1016/j.polymer.2019.03.052.
- [57] B. J. Li, Y. J. Luo, and J. Zheng, “Effect of molecular weight on crystallization and rheological properties of poly(3,3-bis(azidomethyl)oxetane),” *Polym. Sci. Ser. A*, vol. 59, no. 3, pp. 301–309, May 2017, doi: 10.1134/S0965545X17030117.
- [58] M. J. Jenkins and K. L. Harrison, “The effect of molecular weight on the crystallization kinetics of polycaprolactone,” *Polym. Adv. Technol.*, vol. 17, no. 6, pp. 474–478, Jun. 2006, doi: 10.1002/pat.733.
- [59] L. Mandelkern, “The Relation between Structure and Properties of Crystalline Polymers,” *Polym. J.*, vol. 17, no. 1, pp. 337–350, Jan. 1985, doi: 10.1295/polymj.17.337.
- [60] A. V. Ivlev *et al.*, “First Observation of Electrorheological Plasmas,” *Phys. Rev. Lett.*, vol. 100, no. 9, p. 095003, Mar. 2008, doi: 10.1103/PhysRevLett.100.095003.
- [61] A. V. Ivlev *et al.*, “Electrorheological Complex Plasmas,” *IEEE Trans. Plasma Sci.*, vol. 38, no. 4, pp. 733–740, Apr. 2010, doi: 10.1109/TPS.2009.2037716.

Appendix A. SINGLE SLIT EXAMPLE

Consider a light beam passing through a single slit which has the property of transmitting only light plane-polarized in a certain direction, say \hat{z} . An incident beam polarized in \hat{z} will be fully transmitted through the slit, while a beam polarized in \hat{y} will be fully absorbed (Fig. A1a). When the incident beam is polarized at an arbitrary angle α , it is experimentally observed that a fraction of the wave energy proportional to $\sin^2\alpha$ passes through and a fraction of energy proportional to $\cos^2\alpha$ is blocked (Fig. A1b). Due to the wave-particle duality of light, one may be interested in a photon-based description of the same process, which requires discretization. Such a description was provided by Dirac in Sec. 2 of [54], where light plane-polarized in a certain direction is described as consisting of photons, each polarized in the same direction.

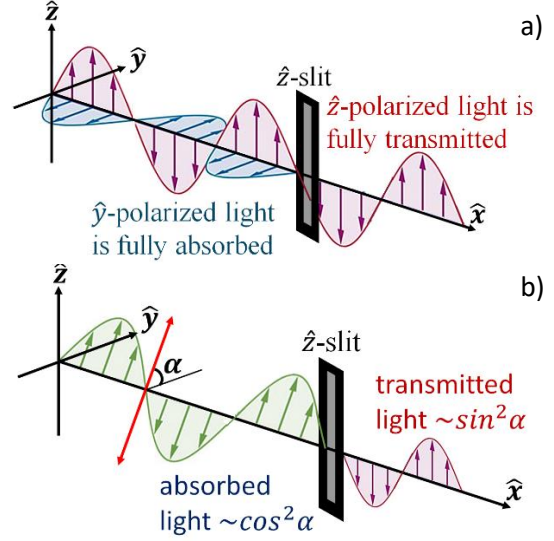


Figure A1. Light transmission through a slit: a) fully absorbed and fully transmitted incident beams and b) α -polarized incident beam.

In the Dirac picture, when an incident beam is polarized in the \hat{z} (or \hat{y}) direction, all of its photons are transmitted (or are absorbed) by the \hat{z} -oriented slit. In the case of obliquely polarized light, where all the photons are polarized at an oblique angle α , it is expected from experiment that a fraction of these photons are still transmitted, even though none of them are initially polarized in the \hat{z} direction. As a photon is the smallest quantum of light, it is not acceptable to have a fraction of a single photon passing through and a fraction being blocked. Therefore, one needs to consider an experiment where a single photon is either transmitted by becoming polarized in \hat{z} direction or is blocked by the slit⁵. If this single photon experiment is repeated many times, it will be found that the number of transmitted photons equals a fraction proportional to $\sin^2\alpha$, while the number of blocked photons equals a fraction proportional to $\cos^2\alpha$. Thus, $\sin^2\alpha$ corresponds to the probability of a photon being transmitted, while $\cos^2\alpha$ is the probability of a photon being blocked by the slit. Conservation of probability is now ensured by the relation $1 = \sin^2\alpha + \cos^2\alpha$. Dirac noted that the values of these probabilities are in excellent agreement with the fractions of wave energies transmitted / blocked in experiments, which validates the description.

Appendix B. NUMERICAL VALIDATION

Section IV presented numerical experiments where we studied transport in disordered media where nonlocal interactions can yield anomalous diffusion. The results demonstrated the possibility of transport enhancement in the regime where different localization mechanisms compete and effectively cancel each other. As these results may have significant physical applications, in this section we examine the various possible sources of numerical errors affecting the computation.

⁵ As noted by Dirac, the purpose of such a description is to explain experimental observations, while preserving the wave-particle duality of light, and not to answer what process flips the polarization of incoming photons as they interact with the slit.

Specifically, we focus on i) statistical fluctuations due to averaging over random realizations of disorder and ii) the effect of truncation on the validity of asymptotic expressions. Instabilities due to loss of orthogonality in the Gram Schmidt procedure are expected to have negligible effect on the results, as discussed in Sec. 4.3 of [20].

1. Randomness of Disorder

Due to the 1D nature of the simulation, it is expected that even small concentrations of random disorder can greatly affect the observed transport behavior. In Sec. IV, we observed that for small disorder concentrations $c \sim 10^{-4}$, we observe the expected behavior of distance plots decreasing faster in the super-diffusive regime and slower in the sub-diffusive regime, when compared to the classical diffusion case. However, once a certain threshold is crossed (resulting in strong localization behavior) it was observed that the anomalous diffusion cases decay more quickly than the classical one (Fig. 6). The deviations from the expected behavior for $c > 10^{-3}$ are due to the nonlocal nature of the fractional Laplacian, which leads to long-range interactions allowing for the propagation of "localization information" at a faster rate as compared to the classical case. Thus, at high concentrations of disorder, the anomalous diffusion distance plots are expected to decay more rapidly in response to the strong localization effect. We expect that this phenomenon would be far less prominent in higher dimensions.

However, in Fig. 9, we observed unexpected de-localization of the distance plots in the sub-diffusive regime at $c = 10^{-3}$ at key combinations of reference lattice scale L and range of nonlocal interaction *range*. The role of truncation at smaller values of *range* is discussed in the next section. To assess the role of randomness in smaller disorder regimes, we performed numerical experiments with the exact parameters as in Fig. 9 but using one order of magnitude smaller disorder $c = 1 \times 10^{-4}$. The results presented in Fig. 10 demonstrate that although transport is naturally enhanced for all realizations in the smaller disorder case, the region $500 < L < 800$ in the sub-diffusive regime (Fig. 10b) still exhibits the unexpected behavior observed in Fig. 9b. This

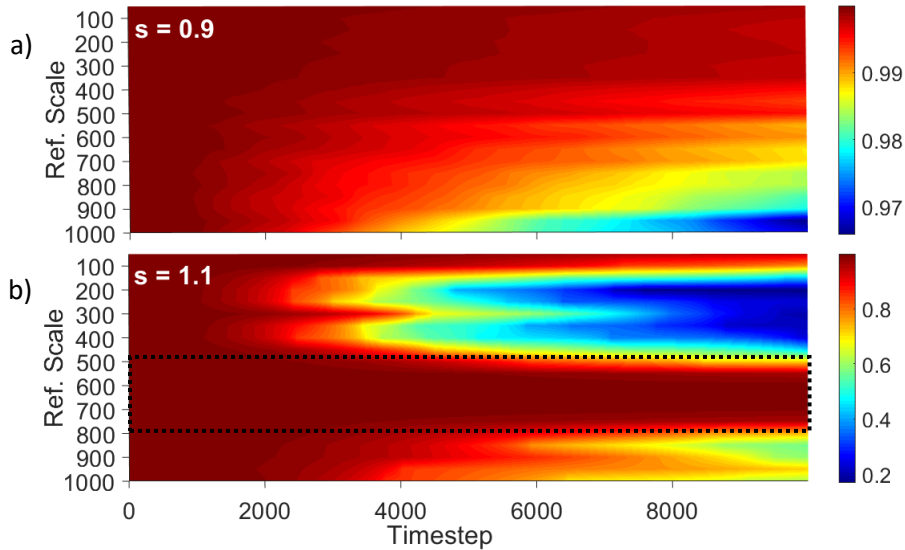


Fig. 10. Time evolution of the distance parameter for increasing reference vector scales in the a) super-diffusive and b) sub-diffusive regimes. All parameters are the same as in Fig. 9 but computed at smaller disorder $c = 1 \times 10^{-4}$. Black dotted contour marks the region where the transport seems to deviate from the expected overall behavior.

suggests that the unusual transport behavior is not caused by the randomness of disorder distribution.

Another test for the role of randomness is to examine how improved averaging affects the outcome of the simulation. In the previous section, we mentioned that each distance plot is an average of 10 realizations of the same numerical experiment, which is needed to minimize fluctuations due to the random realization of the disorder in each individual run. Figure 11 shows the time evolution of the distance plots for the parameters in Fig. 9 in the critical range $400 \leq L \leq 800$ computed using 10 realizations (Fig. 9a) and using 50 realizations (Fig. 9b). As the number of realizations is increased, the enhanced transport behavior is preserved and identified more clearly in the region $550 \leq L \leq 750$. This suggests that averaging over 10 realizations is sufficient to identify interesting features of the transport behavior, which ensures reasonable computation times. However, averaging over larger number of realizations should be used for a more detailed study of interesting regions.

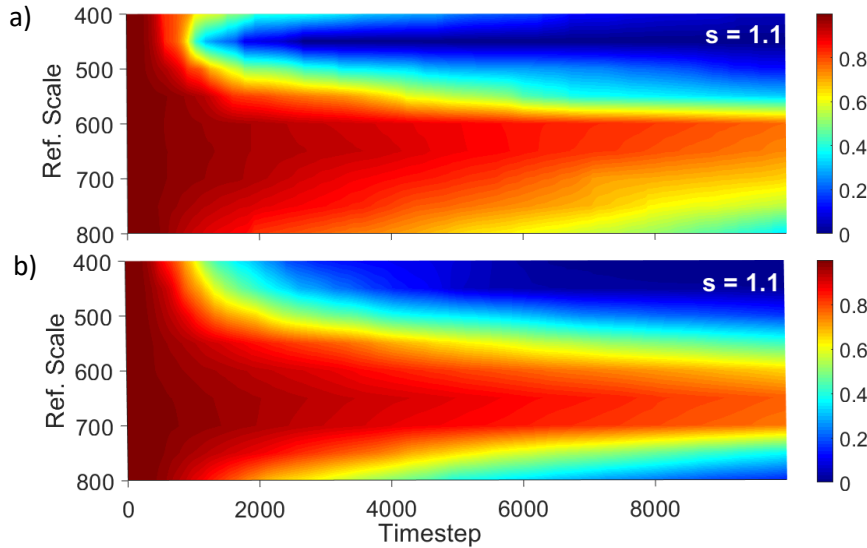


Fig. 11. Time evolution of the distance parameter in the sub-diffusive case for increasing reference scales in the range $400 \leq L \leq 800$ calculated by averaging a) 10 realizations and b) 50 realizations for each set of parameters. All calculations are performed for disorder $c = 1 \times 10^{-3}$ and assuming a fixed range of nonlocal interactions $infl = 300$.

2. Truncation Effects

In addition to randomness, the accuracy of the numerical results can be affected by truncation due to the selected range of nonlocal interactions. In Sec. 2, we introduced the series representation of the fractional Laplacian in equation (4), which we rewrite as

$$(-\Delta)^s u_n = \sum_{m \in \mathbb{N}} (2u_n - u_{n-m} - u_{n+m}) K_s(m), \quad (\text{B1})$$

where the kernel K_s is given by equation (5). This form of the equation is equivalent due to the symmetry of the kernel. Although in the analytical expression the summation goes to infinity, in

the numerical simulation the explicit summation is performed over a finite number of terms, determined by the selected range of nonlocal interactions. Specifically, the numerical equivalent of equation (B1) becomes

$$(-\Delta)^s u_n = \sum_{m=1}^{range} (2u_n - u_{n-m} - u_{n+m})K_s(m) + R_{range}(u_n), \quad (B2)$$

where the remainder is given by

$$R_{range}(u_n) = \sum_{m=range+1}^{\infty} (2u_n - u_{n-m} - u_{n+m})K_s(m) \sim \frac{1}{(range)^2}. \quad (B3)$$

As discussed in Sec. 4 of [20], the remainder is inversely proportional to the square of the range. In the present study, the remainder R_{range} is discarded. Thus, we expect that the numerical results increase in accuracy with increasing *range*. The smallest influence value used in the presented numerical experiments is $range = 50$ (Fig. 7 and 8), which yields the largest remainder $R_{50} \sim 4 \times 10^{-4}$. All other results were obtained using $range = 300$, which yields $R_{300} \sim 10^{-5}$. Even though the remainders are rather small, we acknowledge the possibilities of numerical instability artefacts due to the large timestep used, $\tau = 10,000$.

Deviations from the expected transport behavior may also correspond to some analytical feature of the model. Since expressions related to the fractional Laplacian are exact in the asymptotic limit, it is expected that larger values for *range* (smaller truncation) yield improved results, assuming other numerical instabilities are minimized. For smaller *range* (larger truncation), the calculation using equation (B2) may not be accurate, which would explain the small fluctuations observed in Fig. 7 and 8. However, the unusual de-localization in the sub-diffusive regime in Fig. 9b occurs at large range values, which are expected to yield more accurate results. Finally, the sub-diffusive regime is not as well-behaved as the super-diffusive case due to the lack of a so-called maximum principle. Therefore, further validation of the present numerical results will be sought from exploring alternative implementation methods and comparing with experimental results.